Journal of Power Sources, 43–44 (1993) 277–288

Transition metal displacement in cathodic host structures upon lithium intercalation

R. Brec*, E. Prouzet and G. Ouvrard

Laboratoire de Chimie des Solides, C.N.R.S. (UMR.110), I.M.N., 2 rue de la Houssinière, 44072 Nantes Cedex 03 (France)

Abstract

Reversible intercalation of lithium leads generally to reduction of the transition metal. An instability of the new electronic configuration acquired upon reduction may lead also to its shift to more stable coordination. A transition metal displacement may also take place in order to balance the ionic charge distribution which was disturbed by the reduction (or oxidation) state. These behaviours can explain either the forming (and/or ageing) of cathodic materials or their progressive amorphization.

Introduction

For many years, the intercalation of alkali metals (A) has been studied in transition metal-layered dichalcogenides MX_2 (X being essentially sulfur or selenium). Whereas some intercalates A_xMX_2 present the same structure as the pristine phase, albeit some parameter alterations, others exhibit different arrangements arising from a rigid gliding of the MX_2 layers. Essentially, if the host slabs modify their close-packed stacking, they do so in order to present the suitable, i.e. more stable, coordination and/or bonding around the intercalated species. This coordination change goes from trigonal prismatic to octahedral and, because the MX_2 sandwiches, which contain the strongest ionocovalent bonds, remain unaltered, such a structure modification is well explained in terms of bondings between layers. The resulting new layer stacking is in good agreement with ionicity-structure considerations [1]. For some specific compositions of the intercalates A_xMX_2 ($x=0.25$, 0.33, 0.50...), the interslab cationic repulsion induces particular ordering, in agreement with a higher network ionic energy [2].

The A_xMX_2 intercalate structures are thus clearly related to the guest cation A size, electronegativity and concentration, the host structure itself remaining quasi-unaltered as compared to the pristine layer. This is so because, in agreement with the band structures, reduction of the MX_2 cathodic phase takes place on the M cation which goes from the high oxidation state of (IV), very stable in its environment, to the oxidation state of (III) or more seldom (II), still a fairly-stable state in the same coordination type. It is only recently that drastic host structure modifications involving cationic displacement with or without coordination changes, were recorded on several lithium intercalates. This phenomenon seems to be much more general than originally thought, even in a reversible reaction. This article will describe the transition metal migrations in lithium intercalates, in relation with (i) the modification of the local

*Author to whom correspondence should be addressed.

0378-7753/93/$6.00

ligand field stabilization, and (ii) the modification related to crystal energy minimization. A detailed example of the influence of the transition metal cation diffusion in the host structure upon lithium reduction/intercalation will be given with the cathodic phases $NiPS_3$ and $FePS_3$.

Displacement related to local ligand field stabilization

The case of (2D) 2H–MoS_2

In 2*H*–MoS_2 phase, molybdenum presents a trigonal prismatic (TP) sulfur surrounding, in agreement with the higher stability of Mo(IV) (Fig. 1(a)). The *a'* band is filled and the electron transferred from lithium would be added to a higher energy band (*e'*) (Fig. 1(b)). However, this would lead to strong electronic instability. Consequently, as soon as intercalation occurs, the host structure undergoes a phase transition from prismatic 2*H*–MoS_2 to octahedral 1*T*–MoS_2 (Fig. 2(a)) [3]. The *d* band density of state for this new form of MoS_2 exhibits a low lying T_{2g} band implying a large gain in energy (Fig. 2(b)).

Finally, it appears clearly that the phase transition can be attributed to a drastic increase in the energy of the host cation upon electronic transfer from lithium, the instability created on the Mo(III) cation towards the prismatic environment forcing it to adopt a new and more stable coordination. This is a fine example of ligand field destabilization through a reduction by lithium. It may be thought that the structural transition mechanism is a shear one, involving glide processes between molybdenum and sulfur planes of the same type as the one described for the 1*T* to 2*H* transition in TaS_2 [4]. It is to be noted that one is dealing here with a massive cationic movement, accompanied by a correlative anionic one that starts from the very beginning of intercalation, without a lithium composition threshold triggering the transition.

The first observation of the reverse host metal coordination change from octahedral to trigonal prismatic induced by intercalation was reported for the octahedral host 1*T*–TaS_2, that is for a transition element located on the left of molybdenum. In that case, room temperature sodium and lithium intercalation via an amalgam and via

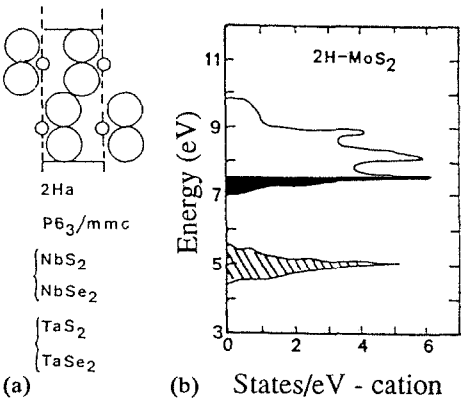

Fig. 1. Schematic representation of the trigonal prismatic sulfur environment of molybdenum in (a) 2*H*–MoS_2 and (b) the corresponding *d* band density of states. The hatched region corresponds to occupied states and the black one to the additional states filled when lithium is intercalated.

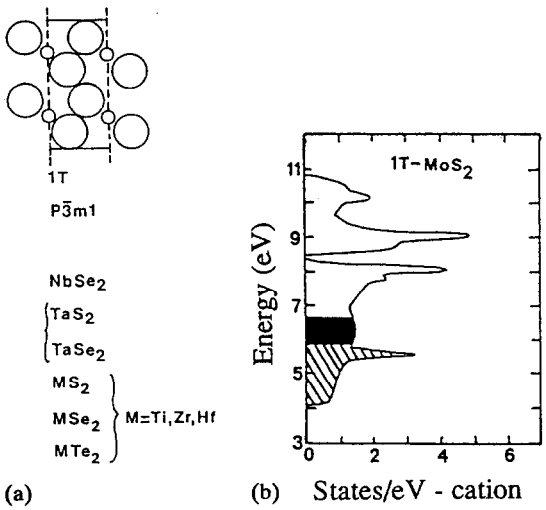

Fig. 2. Schematic representation of the octahedral sulfur environment of molybdenum in (a) hypothetical $1T-MoS_2$ and (b) the corresponding *d* band density of states. The hatched region corresponds to occupied states and the black one to the additional states filled when lithium is intercalated.

butyllithium, respectively, led to the A_x2H–TaS_2 TP polytype [5]. Upon reduction, tantalum goes from *a* d^1 to *a* d^2 electronic configuration, this last one being the same as that of molybdenum in MoS_2, with the same stable TP coordination.

The case of (2D) $NiPS_3$ and $FePS_3$

The MPS_3 phases are derived from the (2D) MX_2 materials by substituting one third of the cations by P_2 pairs according to the sequence:

$$MS_2 \longrightarrow M_{2/3}(P_2)_{1/3}S_2 \longrightarrow M_2P_2S_6 \longrightarrow MPS_3 \qquad (1)$$

These MPS_3 layered-compounds differ from (2D) MX_2 in that the pristine materials show a transition metal at the very low oxidation state of (II), in relation with the highly charged (IV) phosphorus cation, leading to the charge balance: $M^{II}P^{IV}S^{-II}_3$. Since lithium intercalates these phases readily, with the usual charge transfer, one expects a reduction of the M(II) cations to unusually low oxidation states, raising the question of the stability of their new electronic configuration with respect to their pristine environment. It has been demonstrated, through various physical measurements [6] that intercalation in MPS_3 (M = Ni and Fe) occurs according to a bi-electronic transfer, with a reduction of the M(II) cation into M(0) according to:

$$x\mathrm{Li} + M^{II}PS_3 \longrightarrow x/2Li_2M^0PS_3 + (1-x/2)M^{II}PS_3$$

The reaction is bi-phased, as shown by an NMR study of ^{31}P in Li_xNiPS_3 [7] and more recent reassesment of the intercalates X-ray diffraction diagrams [8]. Thanks to the use of the highly accurate and sensitive INEL curve detector which allows, in a capillary Debye–Scherrer geometry and with a monochromated radiation, to obtain well contrasted diagrams of air sensitive phases, it was possible to observe the occurrence of the intercalate phase alongside that of the pristine phase. Figure 3 shows in a 3D representation the progressive growing of the second phase (Li_2NiPS_3 in the case

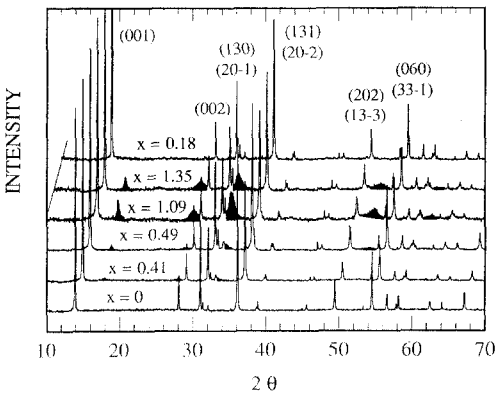

Fig. 3. X-ray diffraction powder pattern of lithium intercalated $NiPS_3$ for various lithium content either at the intercalation or the deintercalation. The black lines correspond to the fully-intercalated phase Li_2NiPS_3.

presented). Although the intensities of the intercalates peaks remain weak and very large, due to their formation at room temperature, the bi-phase nature of the system is clear. Upon deintercalation, the diffraction lines disappear, confirming the already-known reversible character of the Li/MPS_3 system (M = Ni, Fe).

The reduced intercalates are, at least at room temperature, kinetically stable, and their nickel or iron K edge EXAFS spectra could be satisfactorily interpreted as corresponding to a shift of the reduced M(0) species from the initial *Oh* site to an adjacent *Td* one [9, 10]. Let us study the data obtained. In Figs. 4 and 5 the values of $X1$ and $X2$ corresponding to the fraction of atoms respectively in tetrahedral and octahedral environments versus x in Li_xMPS_3 (M = Ni, Fe) are observed. They can be compared with two lines of slope 1/2 (full line) and −1/2 (dotted line) representing the variations of the numbers of reduced and unreduced nickel atoms in the hypothetical above intercalation reaction scheme. It can be observed that the $X1$ values (solid circles on Figs. 4 and 5) fit very well with the solid line, indicating that the transition metals reduced by lithium intercalation move continuously from their initial *Oh* sites to *Td* ones. This behaviour is not really surprising since, in the literature, all the solid-state chemistry examples of nickel or iron in the oxidation state of zero are found in the *Td* environment.

If we consider now the $X2$ values of Figs. 4 and 5 (stars), it can be observed that they follow the dotted line in the case of the iron derivative, but are always situated below this theoretical line in the case of the nickel intercalates, as if there was an extra loss of nickel atoms in the *Oh* sites. This apparent deficiency has been explained by taking into account a first coordination shell of nickel atoms more complex than the one considered in the fits. The EXAFS signals of sulfur and nickel backscatterers are almost in phase opposition. The occurrence of bi-atomic nickel entities in adjacent sulfur tetrahedra decreases the signal attributed to the nickel–sulfur *Oh* environment ($d_{Ni-Ni} = d_{Ni-S} = 2.56$ Å). Because this phenomenon is not observed in Li_2FePS_3, we can conclude that there is an absence of such Fe–Fe entities in the iron intercalate. This difference between the two intercalates is not the only one. In effect, considerations of the second shell (Ni–P, Ni–Ni and Fe–P, Fe–Fe) indicate that the nickel migration takes place exclusively within the $NiPS_3$ slabs, whereas the reduced iron migrates whithin the slab and the van der Waals gap as well.

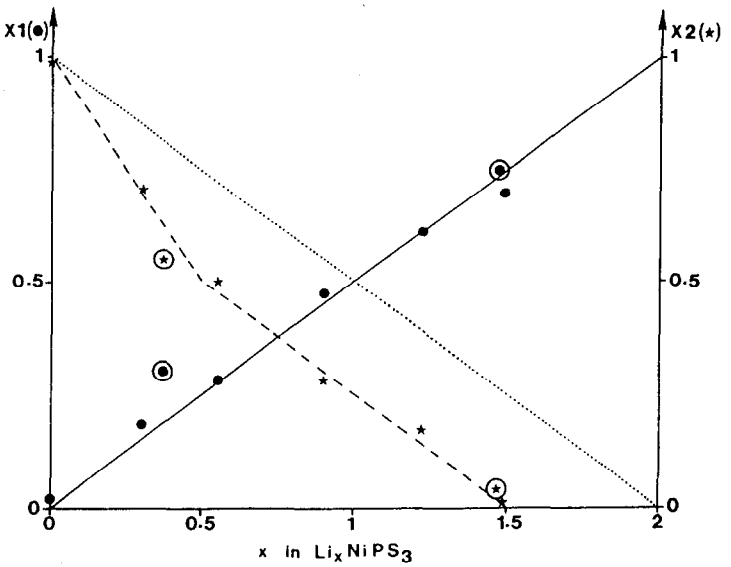

Fig. 4. EXAFS calculated fractions of nickel atoms in tetrahedral (dots) and octahedral (stars) environment in lithium intercalated $NiPS_3$ phase vs. the lithium content. Full line and dotted line represent the theoretical fractions of reduced and unreduced nickel atoms, respectively. Circled values correspond to deintercalated and reintercalated phases.

These results are in accord with the Mössbauer observations indicating [11] that the configurations of Fe(0) in the paramagnetic Li_2FePS_3 is $3d^74s^1$ (and not $3d^8$). This suggest that in Li_2NiPS_3, the diamagnetism of Li_2NiPS_3 is attributed to a similar $3d^94s^1$ configuration (and not $3d^{10}4s^0$), allowing for the Ni–Ni coupling through *d–d* and *s–s* bonding, which is in agreement with the occurrence of a diamagnetic matrix.

In the more simple case of Li_2NiPS_3, a global structure for the intercalate can be put forward, assuming that the $(P_2S_6)^{4-}$ arrangement which characterizes the compound framework remains the same (there is no reason to believe that it changes, the anions remaining untouched by the redox reaction). Figure 6(a) shows a possible coordinated migration of nickel atoms (arrows) and the hypothetical resulting structure of Li_2NiPS_3 is represented in Fig. 6(b). This possible structure maintains the initial frame of $NiPS_3$ with the same *C2/m* space group. It corresponds to the formation of cationic lines along the a parameter with successively a P_2 pair in an octahedron, two nickel atoms in two adjacent tetrahedra, one P_2 pair in an octahedron, and so on.

From the known structure of the MPS_3 phases, the distance between the centre of a tetrahedron and its corners can be estimated equal to 2.15 Å in the slab. The Ni–S and Fe–S fitted distances (2.28 Å) correspond to a volume expansion of tetrahedral sites of about 15%. This is to be compared with the volume of Li_2NiPS_3 cell (419 $Å^3$) and that of $NiPS_3$ (371 $Å^3$) [8].

Upon oxidation, all the metal ions do not move back to their previous *Oh* sites: some remain in their *Td* locations. In the case of $FePS_3$, this transforms the layered phase into a three-dimensional one, whereas the two-dimensional character of $NiPS_3$ is preserved. This probably explains the different electrochemical behaviour of the two phases.

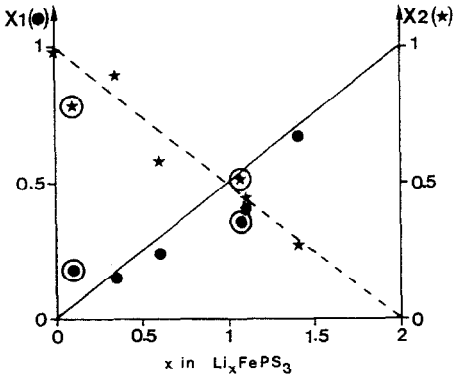

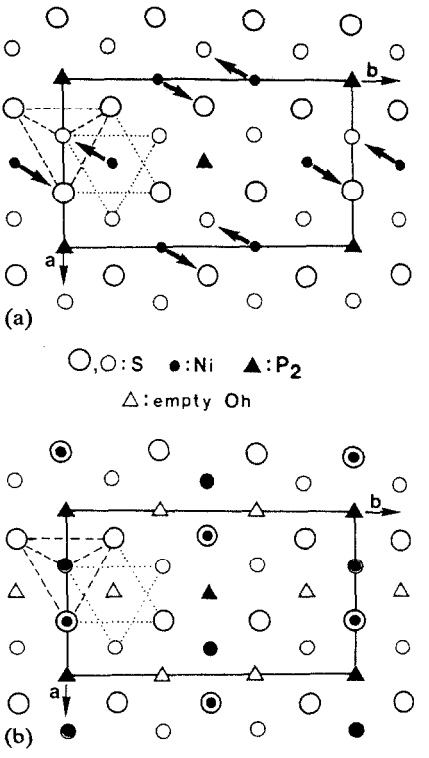

Fig. 5. EXAFS calculated fractions of iron atoms in tetrahedral (dots) and octahedral (stars) environment in lithium intercalated $FePS_3$ phase vs. the lithium content. Full line and dotted line represent the theoretical fractions of reduced and unreduced iron atoms, respectively. Circled values correspond to deintercalated and reintercalated phases.

Fig. 6. (a) Projection perpendicular to the plane of one sheet of $NiPS_3$ in the monoclinic cell. The arrows indicate a possible coordinated migration of nickel atoms in tetrahedral sites in the slab, as deduced from the EXAFS study; (b) resulting hypothetical reduced $NiPS_3$ structure from the displacement of (a). The intercalated lithium atoms have been omitted. Reduced nickel atoms are aligned along the *a*-direction.

These are the two first examples of metals kinetically stable in their elemental state in sulfur coordination in an inorganic compound.

In the above phase, cation displacements were observed on intercalates obtained by a chemical way through the butyllithium technique. An electrochemical intercalation made under high current density, without intermittent relaxation, yields the same data. It had been observed [12] that two different systems (labelled I and II) could be observed for quasi-equilibrium discharge, the first one at high potentials under strict equilibrium conditions, the second at lower voltages when the first discharge was done at a relatively high rate, the following ones being made at equilibrium. In this last experiment, no relaxation of system I would allow it to go back to the higher potential values. These observations could not find a sensible explanation at that time, although they pointed out to the occurrence of two different structures not detected on X-ray diffraction diagrams. A recent EXAFS study [8] of the high potential system have demonstrated that all the nickel atoms in the $Li_{0.55}NiPS_3$ intercalate remain in the

same site and that only a slight increase of the Ni–S distance is observed, in agreement with the larger radius of reduced Ni(0). This means that quasi-equilibrium discharges allow Ni(0) (and also certainly Fe(0) to remain in its pristine site, whereas an initial strong discharge triggers a Ni(0) displacement which continues throughout the structure thereafter, whatever the following relaxation conditions. The curious dual behaviour of $NiPS_3$ and $FePS_3$ intercalated by lithium under different kinetic conditions is thus elucidated.

In other instances, the complete reduction to the zero valence state of the host transition metal may lead to the extraction of the metal in its elemental form. This is mostly the case for the coinage elements copper and silver. For instance, copper is reduced to the metallic state and extruded from the $Cu_xMo_6S_8$ Chevrel phase [13], from the spinel $LiCuVO_4$ [14], according to a mechanism which is reversible. The same phenomenon occurs for silver in $AgV_2O_{5.5}$ [15].

A last example of cationic shift related to local ligand field stabilization can be taken with the reduction of γ–Fe_2O_3 with lithium [16]. A slow scanning voltamperometry

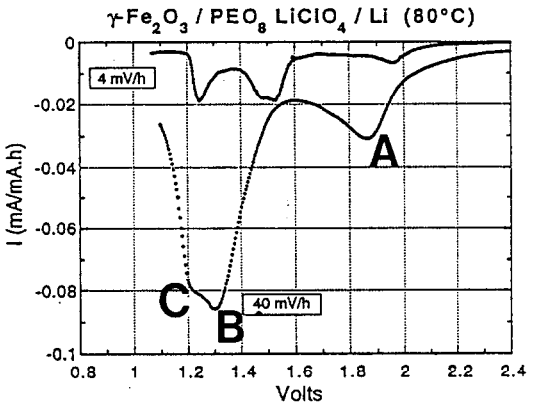

Fig. 7. γ–Fe_2O_3 voltamperometric experiments in $LiClO_4$–PEO at 80 °C (ref. 16).

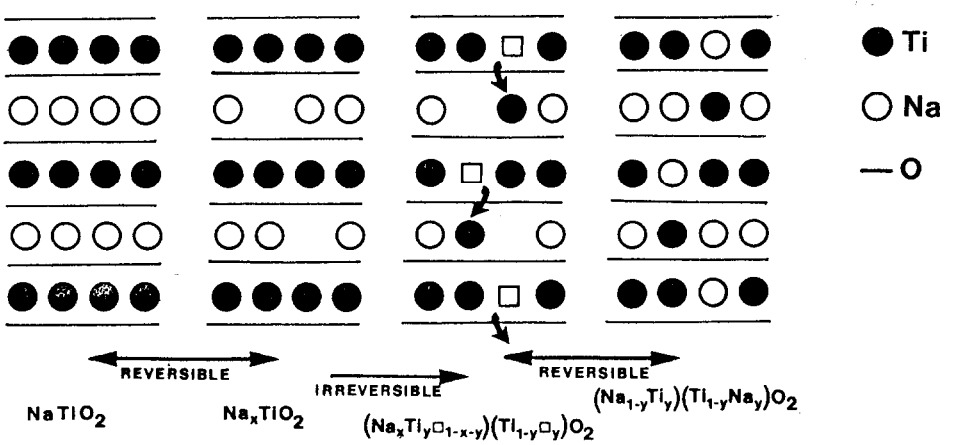

Fig. 8. Reversible and irreversible structural transitions appearing in $NaTiO_2$ at sodium deintercalation. The arrows indicate the irreversible migration of titanium atoms in the van der Waals gap when a large amount of sulfur atoms have been deintercalated.

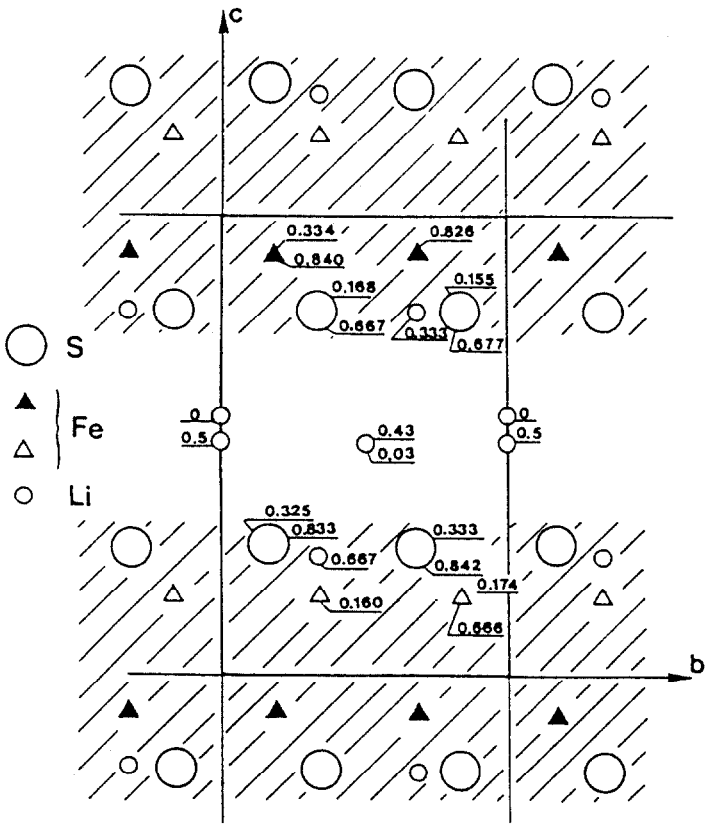

Fig. 9. Projection along the *a*-axis of the Li_2FeS_2 structure. The shaded area underlines the (2D) structure of the FeS_2 framework.

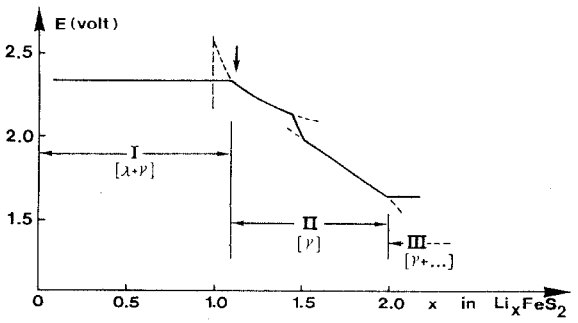

Fig. 10. Open-circuit voltage curve obtained with lithium batteries whose positive electrode is Li_2FeS_2.

made on a Li/$LiClO_4$–PEO / γ–Fe_2O_3 system at 80 °C shows three different reactions corresponding to three current peaks A, B and C (Fig. 7). Peak A ($x=0.30$) can be attributed to the filling of the 1/3 *Oh* voids of the lacunar γ–Fe_2O_3 $((Fe)_{Td}, (Fe_{5/3}\square_{1/3})_{Oh}O_4)$. For peak B, the tangent to the descending peak is independent of

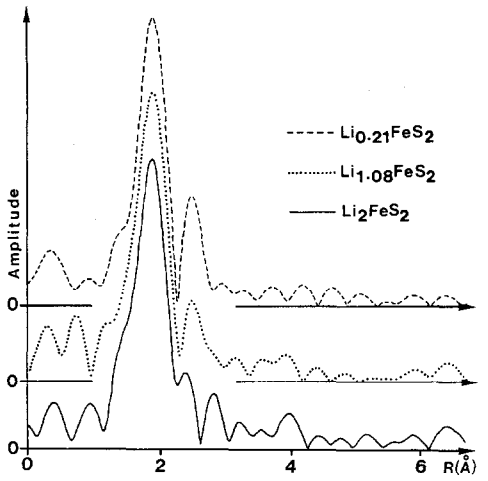

Fig. 11. Fourier transform modules of EXAFS spectra recorded at iron K edge for various compositions in the Li_xFeS_2 system. The curve positions have not been corrected for phase shift.

the sweeping speed indicating a first order transition attributed to the structure change from spinel to a rock salt structure, as shown by the X-ray study. This corresponds to the migration of the *Td* iron cations to *Oh* sites. The transition is slow, in agreement with the type of cationic shift involved. Peak C (at 1.2 V), which position varies little with sweep rates, corresponds to a fast kinetic process and is attributed to the final filling by lithium of the *Oh* sites of lacunar NaCl-type $Li_xFe_2O_3$; the system reaches the composition $LiFe_2O_3$ at the end of peak C. Beyond $x=1$, one observes the final reduction of the Fe^{3+} cations, with an amorphization of the phase. The reduction of Fe^{3+} into Fe^{2+} gives an ion more stable in its high spin *Oh* state, which is achieved by a structural-type first order change. Such transitions had been determined [17, 18] for manganese and iron spinel oxides (M_3O_4) with the same type of cationic shift.

Displacement related to crystal energy minimization

Intercalated transition metal dioxides A_xMO_2

In the A_xMO_2 materials one observes that the host slab presents the same type of arrangement as in the dichalcogenides, with also a very stable highly-oxidized transition metal in octahedral surroundings. The alkali metal ions are intercalated between the adjacent oxygen layers and stabilize the structure through the ionic A–O bonds (Fig. 8). Alkali metal content x in the A_xMO_2 compounds cannot be very low because of the strongly ionic nature of the phases.

When one deintercalates lithium for instance from $LiMO_2$ systems (with a *O*3-type), non-stoichiometric Li_xMO_2 phases are obtained reversibly down to $x=0.5$, 0.5 and 0.7 for cobalt, nickel and vanadium respectively [19–21]. In these reversible domains, no structural modification is recorded. For lower lithium content, however, some M atoms leave the slabs and migrate to the interstitial space (Fig. 8), the Li_xMO_2 domains becoming nonreversible. Such 2D → 3D structural transitions are common to most A_xMO_2 systems. In these cases, because the cations are stable in their (III) and (IV) oxidation state in *Oh* environment, the metal displacement is only to be attributed

TABLE 1

Examples of phases where transition displacements for transition metal atoms can be observed when alkali metal atom is intercalated or deintercalated. Distinctions have been made between both origins of the stabilization process

Compounds	Redox reaction ⟨1⟩ monophased ⟨2⟩ biphased	LFS or CEM[a]	ME[b]	Ref.
MoS_2 Type of displacement	⟨2⟩ $x\text{Li} + MoS_2 \Longleftrightarrow x\text{LiMoS}_2 + (1-x)MoS_2$ $TP \longrightarrow Oh$ $Mo^4 + (4d^2) \longrightarrow Mo^{3+}(4d^3)$	LFS	No	3
TaS_2 Type of displacement	⟨2⟩ x(Li or Na) $+ TaS_2 \Longleftrightarrow$ (Li or Na)$_x TaS_2$ $Oh \longrightarrow TP$ $Ta^{4+}(5d^1) \longrightarrow Ta^{3+}(5d^2)$	LFS	No	5
MPS_3 (M = Ni, Fe) Type of displacement	⟨2⟩ $x\text{Li} + MPS_3 \Longleftrightarrow (x/2)\text{Li}_2MPS_3 + (1-x/2)MPS_3$ $Oh \longrightarrow Td$ $Fe^{2+}(3d^6s^0) \longrightarrow Fe^0(3d^74s^1)$ $Ni^{2+}(3d^84s^0) \longrightarrow Ni^0(3d^94s^1)$	LFS	No	8–10
$AgV_2O_{5.5}$	⟨2⟩ $x\text{Li} + AgV_2O_{5.5} \Longleftrightarrow x(\text{LiV}_2O_{5.5} + \text{Ag}) + (1-x)AgV_2O_{5.5}$	LFS	Yes	15
$Cu_2V_2O_7$	⟨2⟩ $x\text{Li} + Cu_2V_2O_7 \Longleftrightarrow x/2(\text{Cu} + 1/2\text{Li}_4V_2O_7) + (1-x/4)Cu_2V_2O_7$	LFS	Yes	24
$M_xMo_6S_8$ (M = Cu, Ag, In, Tl)	⟨2⟩ $x\text{Li} + M_yMo_6S_8 \Longleftrightarrow x\text{M} + \text{Li}_xM_{(y-x)}Mo_6S_8$	LFS	Yes	13
$LiCuVO_4$	⟨2⟩ $x\text{Li} + \text{LiCuVO}_4 \Longleftrightarrow x(\text{Cu} + \text{Li}_2\text{CuVO}_4) + (1-x)\text{LiCuVO}_4$	LFS	Yes	14
γ-Fe_2O_3 Defect spinel Type of displacement	⟨1⟩ or ⟨2⟩ $x\text{Li} + Fe_2O_3 \Longleftrightarrow \text{Li}_xFe_2O_3$ (spinel $\longrightarrow$ NaCl for $x > 0.25$) $Td \longrightarrow Oh$ $Fe^{3+}(3d^5) \longrightarrow Fe^{2+}(3d^6)$	LFS	No	16
M_3O_4 spinel (M = Mn, Fe) Type of displacement	⟨1⟩ $x\text{Li} + M_3O_4 \Longleftrightarrow \text{Li}_xM_3O_4$ $Td \longrightarrow Oh$ $Fe^{3+}(3d^5) \longrightarrow Fe^{2+}(3d^6)$ $Mn^{3+}(3d^4) \longrightarrow Mn^{2+}(3d^5)$	LFS	No	17, 18
A_xMO_2 M = Co, Ni, V... A = Li, Na, K Type of displacement	⟨2⟩ $AMO_2 \Longleftrightarrow A_{(1-x)}MO_2 + x\text{A}$ $M^{3+}{}_{(Oh)} \longrightarrow M^{4+}{}_{(Oh)}$	CEM	No	19–21
Li_xFeS_2 Type of displacement	⟨1⟩ $\text{Li}_2FeS_2 \Longleftrightarrow \text{Li}_{(2-x)}FeS_2 + x\text{Li}$ $Fe^{2+}{}_{(Td)} \longrightarrow Fe^{3+}{}_{(Td)}$	CEM	No	22, 23
$CuFeS_2$ Type of displacement	⟨1⟩ $\text{LiCuFeS}_2 \Longleftrightarrow \text{Li}_{1-x}\text{CuFeS}_2 + x\text{Li}$ $Cu^{+}{}_{(Td)} \longrightarrow Cu^{2+}{}_{(Td)}$	CEM	No	25

[a]LFS: ligand field stabilization, CEM: crystal energy minimization.
[b]ME: metal extrusion.

to the Madelung energy minimization. One can point out that these cationic shifts take place at threshold values, probably in relation to the activation energy of the phenomenon and the electronegativity of M (the threshold is higher in the case of the more electronegative vanadium for instance).

The case of the Li_xFeS_2 system

Li_2FeS_2 is a ternary sulfide which structure [22] is made of hexagonal close packing layers of S(−II) with iron ions Fe(II) in tetrahedral coordination in every other slab. Between the (SFeS) layers lithium is found in tetrahedral and octahedral sites (Fig. 9). Because of its mobility, lithium can be removed from the host lattice, and in the high lithium content region ($1<x<2$), the Li_xFeS_2 system is another example of a structural change related to crystal energy minimization. Lithium removal from Li_2FeS_2 to $LiFeS_2$ results in the oxidation of Fe(II) to Fe(III), the cell size changing very little. However a break is observed for $x=1.5$ on the equilibrium recharge (or discharge) curve of a Li_xFeS_2/Li battery (Fig. 10). An EXAFS study performed, at the iron K edge, on a Li_xFeS_2 series, shows that there is no change in the first iron shell, which remains a sulfur tetrahedral coordination [23] (Fig. 11). A Mössbauer analysis indicates that, around the $Li_{1.5}FeS_2$ composition, the characteristics of one of the two tetrahedral iron sites change drastically, while showing the expected isomer shift for a still tetrahedral species. All these facts indicate that, although less ionic in nature than the oxide phases, this sulfide undergoes the same type of charge redistribution to achieve crystal energy minimization upon insertion or removal of lithium. The coordination of the cationic host is maintained and only its location is modified to compensate for the lithium charge distribution change. Again in that example, the phenomenon takes place at a specific threshold value ($x=1.5$), with a massive cation displacement, in contrast with the continuous transition of Li_xNiPS_3 and Li_xFePS_3.

Conclusion

As gathered in Table 1, more and more examples are now known, in which lithium intercalated/deintercalated compounds experience an important transition metal displacement. This phenomenon is not always clearly observed because the X-ray diffraction patterns do not necessarily represent the important and easily detectable changes. Local structure analyses are a more powerful tool in these cases. These cationic displacements have important consequences on the positive electrode and discharge/charge regime of the lithium cells (higher or lower plateaus, curve drops). The host metal shifts can be attributed mainly to a change in the cation local stability, a long-range crystal stability (Madelung energy) or both. In the extreme cases of the coinage elements, copper and silver, the reduction and displacement processes may lead to the reversible or nonreversible extruding of these host metals.

References

1 J. Rouxel, *J. Solid State Chem., 17* (1976) 223.
2 P. Deniard, *Ph.D. Thesis*, University of Nantes, France, 1988.
3 M. A. Py and R. R. Haering, *Can. J. Phys., 61* (1983) 76.
4 J. van Landuyt, G. van Tendeloo and S. Amelinckx, *Phys. Status Solidi A, 26* (1974) 585.
5 P. Ganal, W. Olberding, T. Butz and G. Ouvrard, *Solid State Ionics,* to be submitted.

6 R. Brec, *Solid State Ionics, 22* (1986) 3.
7 Y. Chabre, P. Segransan, C. Berthier and G. Ouvrard, in P. Vashishta, J. N. Mundy and G. K. Shenoy (eds.), *Fast Ion Transport in Solids*, North-Holland, Amsterdam, 1979, p. 221.
8 E. Prouzet, G. Ouvrard, P. Fragnaud and R. Brec, *J. Solid State Chem.*, to be submitted.
9 G. Ouvrard, E. Prouzet, R. Brec, S. Benazeth and H. Dexpert, *J. Solid State Chem., 86* (1990) 238.
10 G. Ouvrard, E. Prouzet, R. Brec and H. Dexpert, *J. Solid State Chem., 91* (1991) 271.
11 G. A. Fatseas, M. Evain, G. Ouvrard, R. Brec and M. H. Whangbo, *Phys. Rev. B, 35* (1987) 3082.
12 G. Ouvrard, *Ph.D. Thesis*, University of Nantes, France, 1980.
13 Y. Yakeda, R. Kanno, M. Noda and O. Yamamoto, *Mater. Res. Bull., 20* (1985) 71.
14 R. Kanno, Y. Takeda, M. Hasegawa, Y. Kawamoto and O. Yamamoto, *J. Solid State Chem., 94* (1991) 319.
15 E. S. Takeuchi and W. C. Thiebolt, III, *J. Electrochem. Soc., 135* (1988) 2691.
16 Y. Chabre, *Chemical Physics of Intercalation II, June 28–July 8, 1992, Bonasse, France, NATO-ASI Ser.*, in preparation.
17 M. M. Thackeray, W. I. F. David and J. B. Goodenough, *Mater. Res. Bull., 17* (1982) 785.
18 M. M. Thackeray, W. I. F. David, P. G. Bruce and J. B. Goodenough, *Mater. Res. Bull., 18* (1983) 461.
19 L. A. de Picciotto and M. M. Thackeray, *Mater. Res. Bull., 19* (1984) 1497.
20 K. Mizushima, P. C. Jones, P. J. Wiseman and J. B. Goodenough, *Mater. Res. Bull., 15* (1980) 783.
21 M. G. Thomas, W. I. David, J. B. Goodenough and P. Groves, *Mater. Res. Bull., 20* (1987) 1137.
22 L. Blandeau, G. Ouvrard, Y. Calage, R. Brec and J. Rouxel, *J. Phys. C, 20* (1987) 4271.
23 R. Brec, E. Prouzet and G. Ouvrard, *J. Power Sources, 26* (1988) 325.
24 Y. Sakurai, H. Ohtsuka and J. Yamaki, *J. Electrochem. Soc., 135* (1988) 22.
25 R. Fong and J. R. Dahn, *Phys. Rev. B, 39* (1989) 4424.